J Mater Sci: Mater Electron (2023) 34:1312

Investigation of the structural and temperature-dependent electrical properties of MZnO (M = Ce and Sm) Schottky diode devices fabricated using the sol–gel spin-coating technique

Mustafa A. M. Ahmed[1,2,*] , W. E. Meyer[1], and J. M. Nel[1]

[1] *Department of Physics, University of Pretoria, Private Bag X20, Hatfield 0028, South Africa*
[2] *Department of Physics, Faculty of Education, University of Khartoum, P.O Box 321, Omdurman 11115, Sudan*

Received: 22 February 2023
Accepted: 11 May 2023
Published online:
9 June 2023

© The Author(s) 2023

ABSTRACT

In the present study, the Schottky diode devices based on Ce and Sm co-doped ZnO thin films were fabricated using the sol–gel spin-coating technique with Pd and Pt as Schottky contacts. The structural and electrical properties of the fabricated Schottky diode devices were investigated at room temperature and in the temperature range of 320–160 K. The crystalline structure of the prepared films was studied using X-ray diffraction spectroscopy. The *I–V* characteristics of the fabricated Schottky diode devices based on Pd and Pt Schottky contacts manifest good diode behavior with the rectification of nine and ten orders of magnitudes, respectively. The ideality factor for Pd-based Schottky diode was found to decrease with temperature, and the lowest value obtained at 160 K was 1.3, while for the Pt-based Schottky diode, the ideality factor was found to increase with decreasing temperature. Moreover, by using two Gaussian models, the barrier height for Pt Schottky diodes was found to decrease with decreasing temperature indicating the inhomogeneity in the barrier height. Furthermore, alongside the thermionic emission theory, the fabricated Schottky diode parameters were also analyzed with Cheung–Cheung and the modified Nord methods. Finally, the current transport mechanism in both fabricated Pd and Pt was found to be controlled by an Ohmic, trap-filled voltage and space-charge-limited current mechanisms in the low, moderate and higher voltage bias, respectively.

Address correspondence to E-mail: mustafa.sonbl@gmail.com

https://doi.org/10.1007/s10854-023-10621-5

1 Introduction

Zinc oxide (ZnO) is one of the promising environmentally friendly semiconductor materials having a direct wide band gap (3.37 eV) and large exciton energy (60 meV) at room temperature which makes it well suited for use in optoelectronic devices performing in near ultraviolet (UV) [1–4]. Among ZnO nanostructures such as nanorods, nanoflowers, and nanowires, ZnO thin films have been studied extensively in recent years due to their wide range of application in electronic devices such as light-emitting diodes [5, 6], solar cells [7], gas sensors [8], UV lasers transparent conductive films [9], and Schottky diode devices [10–14]. ZnO has superior physical properties such as high electron saturation velocity, high breakdown electric field, radiation tolerance, and high thermal conductivity, which are comparable to the other conventional wide band gaps semiconductors such as GaN and SiC, and are also better than those of GaAs and Si [15, 16].

The physical and chemical properties of ZnO semiconductor material can be altered by doping it with some cations. Transition metals such as Al, Ag, Mn, and Co have been used and studied as effective dopants for ZnO thin films [17–20]. Rare-earth (RE) metals such as La, Ce, Sm, Eu, Er, and Yb have also been used as dopants for ZnO to improve its optical and electrical properties [21–25]. The availability of 4*f* electrons and their fluorescence efficiency results in good optical and electrical properties [26]. Among these RE metals Ce and Sm have been studied extensively and have been shown to be good candidates for ZnO dopants due to their optical and electrical properties [22, 23, 27]. Recently, Ce- and Sm-doped and co-doped ZnO thin films have produced good Schottky diode devices at room temperature with ideality factor near to the unity using Pd as the Schottky contact [28, 29]. Moreover, a combination of Al and Ce co-doped ZnO thin films have also shown to manifest good optical and electrical properties as reported in [30].

Obtaining good rectifying Schottky contacts on ZnO is difficult to achieve because of the formation of an oxide layer between Si and ZnO. Therefore, treatment is needed prior to contact fabrication. This can be done by chemical cleaning using hydrogen peroxide, hydrofluoric acid, or by plasma treatment. Fabrication of high-quality metal/ZnO Schottky diode devices has been of substantial interest to the research community. In general, the reliability and performance of metal–semiconductor device are affected by the quality of the fabricated contact between metal and semiconductor. This is due to the fact that Schottky barrier height which controls the transport properties is given by the difference between the majority charge carrier's energy levels across the metal–semiconductor interface [31]. Under applied different bias and temperatures, the Schottky barrier height was found to differ as observed in GaAs and ZnO [16, 32, 33]. Moreover, the variation of temperature can also affect the Schottky barrier heights which in turn influence the device performance as reported in [16]. Moreover, the device characteristics can also be affected by the formation of oxide layers and interface states which results in deviation from the ideal behavior of the diode.

Synthesis of ZnO thin films has been done using a variety of techniques including, spray pyrolysis [34], metalorganic chemical vapor deposition [35], molecular beam epitaxy [36], pulsed laser deposition [37], and the sol–gel spin-coating techniques [38–41]. In this study, the sol–gel spin-coating technique was used to synthesize the Ce- and Sm-co-doped ZnO thin films, due to its simplicity and adaptability of the experimental setup, low cost, low-temperature crystallization, and homogeneity of the produced films. Using the sol–gel spin-coating methods, Ce and Sm co-doped ZnO films were deposited on glass and n-Si substrates. Deposited films on glass substrates were used for structural and optical characterization, while films deposited on n-Si substrates were used for device fabrication and characterization. As we mentioned earlier, Ce and Sm have shown to be a good candidates as a dopant for ZnO Schottky diode devices at room temperature [28, 29]. However, to the best of our knowledge, no reports are available on temperature-dependent electrical properties of the fabricated Ce and Sm co-doped ZnO thin films using the sol–gel spin-coating methods. Therefore, in this study, we fabricated Ce- and Sm-co-doped ZnO thin films Schottky diode devices using Pd and Pt Schottky contacts. The structural properties of the prepared films were studied at room temperature and the electrical properties of the fabricated Schottky diode devices based on Pd and Pt Schottky contacts were investigated in detail in the temperature range 320–160 K, and have shown good Schottky behavior with a rectification being nine and ten orders of magnitude, respectively.

2 Experimental methods

2.1 Materials

In these experiments, the following raw materials were used as purchased without any further purification, namely: zinc acetate dihydrate (98%, Merck), monoethanolamine (MEA) (98%, Merck), iso-propanol (99.95%, Merck), cerium nitrate hexahydrate (99.999%, Sigma Aldrich), and samarium nitrate hexahydrate (99.9%, Sigma Aldrich).

2.2 Preparation and deposition of Sm- and Ce-doped and co-doped ZnO thin films

ZnO sol–gel solution was prepared by dissolving zinc acetate dihydrate into 60 ml iso-propanol which was stirred for 1 h at 500 rpm and 60 °C. Thereafter, MEA in a 1:1 molar ratio with the zinc acetate was added drop-wise to the solution as a stabilizer while continuously stirring under the same conditions for 1 h. Doping was performed by adding 2 at.% of cerium nitrates and 2 at.% samarium nitrates to the above solution following the same procedures used to ZnO sol–gel. The transparent, clear solution was then aged for 96 h prior to the deposition, to increase the viscosity of the gels. Before the deposition, glass substrates were cleaned with deionized water, ethanol, acetone, and deionized water, in this sequence for 15 min in an ultrasonic bath, and finally blown dry with nitrogen gas. Si substrates were cleaned following the procedures explained elsewhere [42]. Aged sol–gels were then spin coated on pre-cleaned glass and Si substrates 3 layers (i.e., Ce and Sm-doped ZnO solution) at 3000 rpm for 30 s, thereafter drying in an oven preheated at 200°C for $\sim$5 min. This process was repeated until the desired thickness was obtained. Finally, the coated substrates were dried at 250 °C for 5 min to remove any remaining organic residuals. Prior to characterizations, coated films on glass and Si substrates were annealed at 450 °C in Ar gas for 1 h with a temperature ramped at a rate of 10 °C/ min.

2.3 Contacts fabrication

For device fabrications, two deposition systems were used in this study namely, the resistive evaporation and electron beam deposition (e-beam). The substrate used for device fabrication was n-type Si (111) (13–17 μm and 1.4–1.8 Ω.cm) which was diced into small pieces, and divided into two sets. For the first set, Pd and Au-Sb were used as the Schottky and Ohmic contacts, respectively. 150 nm of Au-Sb alloy contact was resistively evaporated onto the back side of the Si substrate. The evaporated AuSb layer was immediately annealed at 375 °C for 10 min under flowing Ar prior to spin coating the sol–gel onto the other side of the Si substrate. 100-nm-thick circular Pd contacts were used as a Schottky contact evaporated resistively on the annealed thin films. The ohmic and Schottky contacts were deposited at a deposition rate of 0.1 nm/s and a vacuum chamber's pressure of 3.5×10^{-6} mbar. In the second set, the Schottky and Ohmic contacts were Pt and (Ti/Al), respectively, with a relative thickness of 50 and (20/80) nm, evaporated using an e-beam. A mechanical shadow mask with 0.8-mm-diameter holes was used to evaporate Pd and Pt Schottky contacts. The pressure of the e-beam chambers was below 1×10^{-6} mbar. The deposition rate for Ti and Al were 0.3 Å/s and 1.3Å/s, respectively. Furthermore, both ohmic contacts deposited with resistive and e-beam systems were annealed under flowing of Ar gas for 10 min. Finally, the ohmic contacts deposited with the resistive evaporator and e-beam were onto the unpolished side of the Si substrate. It should be mentioned that both ohmic contacts have shown more less similar resistance and reverse current at room temperature. A schematic drawing of the fabricated Schottky devices is shown in Fig. 1.

3 Characterization

The polycrystalline Ce and Sm-co-doped ZnO thin films were characterized in terms of their morphological and structural properties by a Zeiss crossbeam 540 field emission gun scanning electron microscope (FESEM) and a Rigaku SmartLab X-ray diffractometer (XRD) with $\lambda = 1.54059$ nm, respectively. Finally, the current–voltage (I–V) characteristics of the fabricated Ce and Sm-co-doped ZnO Schottky diodes were studied with the current–voltage (*I–V*) using SMU (Keithly B2912A) 230 m in the temperature range 320 to 160 K.

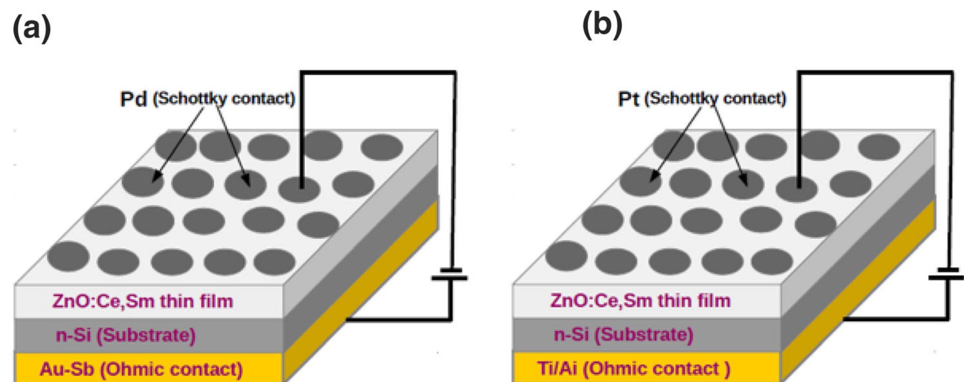

Fig. 1 Schematic diagram of the fabricated Schottky diodes based on the Ce and Sm co-doped ZnO thin films using **a** Pd and **b** Pt as a Schottky contact

4 Results and discussion

4.1 Structural and morphological results

The SEM image of the deposited Ce and Sm-co-doped ZnO thin films is shown in Fig. 2a. The image shows uniform films with particle sizes in the range of 50–100 nm. From the histogram analysis of the morphology images, the average crystallite size was found to be 60 nm. Figure 2b represents the XRD pattern of the prepared Ce and Sm-co-doped ZnO thin films measured at room temperature. The observed peaks could be assigned to the wurtzite ZnO structure with one small peak due to cerium dioxide. From the relative intensities of XRD peaks, the films are polycrystalline in nature, and the preferred orientation of the films is along the (002) plane. The presence of a small cerium dioxide peak revealed that the cerium dopant had exceeded its solubility limit. The observed cerium dioxide peak in the XRD pattern is similar to the previously reported by [30, 43]. No other peaks related to Sm or samarium oxide have been observed in the XRD pattern. This result indicates that the Sm dopant has been successfully incorporated into the ZnO lattice. Moreover, the XRD pattern obtained for the Ce and Sm-co-doped ZnO thin films is in agreement with JCPDS #00 – 036 – 1451. The calculated crystallographic properties presented in this work are similar to previously reported [30]. The calculated lattice parameters are in good agreement with JCPDS #00 – 036 – 1451. Furthermore, our calculated lattice parameters are different from the previously reported Ce- and Sm-co-doped ZnO thin films annealed at

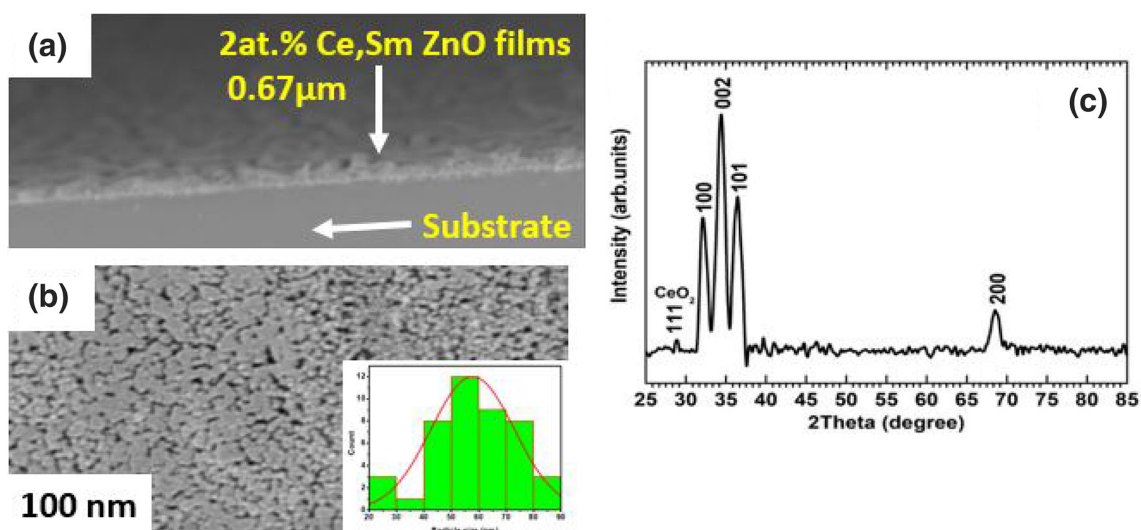

Fig. 2 **a** and **b** are the SEM cross-sectional view and surface morphology images of Ce and Sm-co-doped ZnO thin films, respectively. **c** The XRD pattern of Ce and Sm-co-doped ZnO thin films annealed at 450 °C underflow of Ar gas. The inset depicts the histogram analysis of the SEM image

500 °C ($a = b = 3.311$ Å and $c = 5.163$ Å) [28]. This could be attributed to the different annealing atmospheres and temperatures. In our previous work, the deposited Ce- and Sm-co-doped ZnO films were annealed at 500 °C in air for 1 hr, while in the present study, our deposited films are annealed at 450 °C in an Ar gas for 1 hr.

The average crystallite size D of the prepared Ce and Sm-co-doped ZnO films for the (101), (002), and (200) was calculated using the Debye-Sherer formula [44, 45]:

$$D = \frac{K\lambda}{\beta cos\theta}, \quad (1)$$

where K is the Scherrer constant (here we used $K = 0.9$), λ is the wavelength, β is the full width at half maximum, and θ is the Bragg angle. The calculated D values (tabulated in Table 1) are in good agreement with those obtained from SEM analysis. Furthermore, the volume of the unit cell was calculated as illustrated in Ref. [46].

4.2 Electrical characterization of Pd/ZnO:Ce,Sm/n-Si/AuSb, and Pt/ZnO:Ce,Sm/n-Si/Ti/Al Schottky diodes

Figure 3a and b depicts the I--V characteristics of the fabricated Ce and Sm-co-doped ZnO thin-film Schottky diode devices based on two Schottky contacts namely, Pd and Pt with the structure Pd/CeSmZnO/n-Si/AuSb and Pt/CeSmZnO/n-Si/Ti/Al, respectively. The measurements were performed in the temperature range of 320–160 K. The rectifying behavior of both Schottky diodes improved with decreasing the temperature (see Fig. 3). This indicates that there is strong temperature dependent for both fabricated Schottky diode devices. Note that, at very low temperatures, the reverse current in both I–V characteristics decreases below the measurement capabilities of the system. This is more pronounced in the case of the Pd Schottky diode devices below the measurement capabilities of the system. This is more pronounced in the case of the Pd-based Schottky contacts (see Fig. 3a). The rectification orders for Pd- and Pt-based Schottky diode devices in the temperature range 320 to 160 K were found to be approximately nine and 10 orders of magnitude, respectively. To analyze the I–V characteristics of the fabricated Schottky diode devices, the conventional thermionic emission theory was used without considering the effect of the series resistance (for now) [47]:

$$I = I_s\left[\exp\left(\frac{(qV - IqR_s)}{k_\beta T}\right) - 1\right], \quad (2)$$

where q represents the electronic charge, V is the applied voltage, R_s is the series resistance, and I_s is the saturation current in the absence of external bias, and is given by the following equation:

$$I_s = AA^*T^2\exp\left[\frac{-q\Phi_{B_0}}{k_\beta T}\right], \quad (3)$$

where A^* is the effective Richardson constant (32 $Acm^{-2}K^{-2}$ for ZnO), A represents the contact area of the diode ($\approx 2.83 \times 10^{-3}$ cm^2), Φ_{B_0} is the Schottky barrier height at zero bias, k_β is the Boltzmann constant, T is the absolute temperature, and n is the diode's ideality factor. The zero bias barrier height is calculated as $(kT/q)\ln(AA^*T^2/I_s)$ and the ideality factor is calculated by $n = q/k_\beta T[dV/d(lnI)]$, where $n = 1$ for an ideal diode. The evaluated parameters for both fabricated Pd and Pt-based Schottky diodes are obtained from a linear fit to the I–V curves in the forward bias using Eq. 2 and Eq. 3. The results are summarized in Table 2 and 3, respectively.

In the case of the Pd Schottky contact, both the ideality factor and series resistance show a temperature dependence as depicted in Fig. 4a and Table 2,

Table 1 Crystallographic properties: lattice constants, peak position (2θ), FWHM, particle size (D), and volume of the unit cell (V) of as-synthesized annealed at 500 °C

2%	Lattice constant (Å)		2θ (degree)			FWHM (degree)			D (nm)			V
CeSmZnO	a	c	(100)	(002)	(101)	(100)	(002)	(101)	(100)	(002)	(101)	(Å^3)
	3.220	5.210	32.12	34.40	36.45	0.97	1.18	1.80	70	81.6	55	47

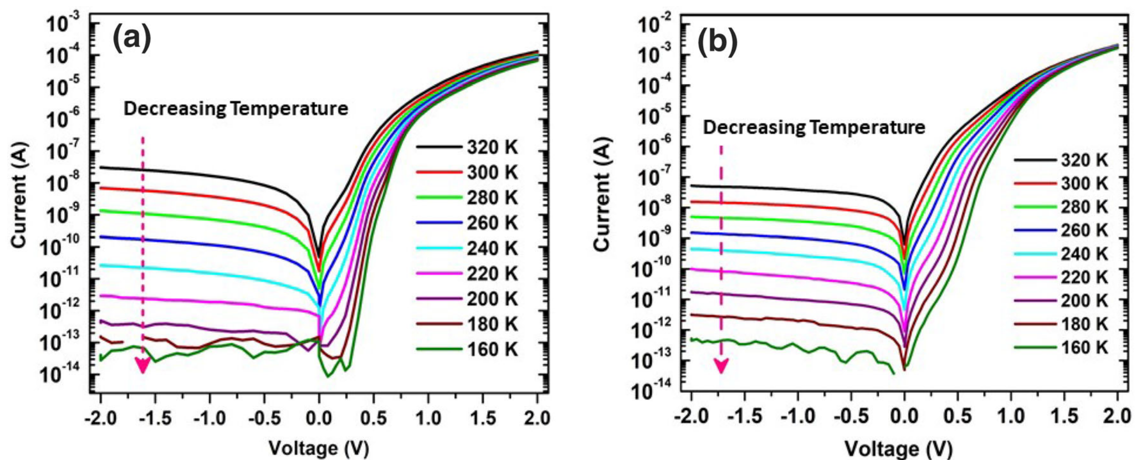

Fig. 3 I–V characteristics of the Ce- and Sm-co-doped ZnO thin films Schottky diode devices based on **a** Pd/CeSmZnO/n-Si/AuSb and **b** Pt/CeSmZnO/n-Si/Ti/Al Schottky contacts in the temperature range 320 to 160 K

Table 2 Schottky diodes parameters of the Pd/Ce,Sm:ZnO/n-Si/AuSb evaluated using the conventional ln I vs. V, Cheung and Nord methods

T	ln I vs. V			$d(V)/d(\ln I)$		H(I)		Nord				
	n	Φ_{B_0}	R_s	n	R_s	R_s	Φ_{cheu}	I_0	V_0	$F(V_0)$	R_s	Φ_N
(K)		(eV)	($k\Omega$)	n	($k\Omega$)	($k\Omega$)	(eV)	(A)	(V)	(V)	(Ω)	(eV)
320	2.57	0.67	4.70	6.66	4.68	4.74	0.72	2.6×10^{-7}	0.48	0.834	5k	0.97
300	2.45	0.74	5.40	7.51	4.52	4.51	0.67	1.0×10^{-7}	0.48	0.804	111k	0.94
280	2.34	0.75	6.00	8.30	4.38	4.33	0.63	6.6×10^{-8}	0.48	0.772	242k	0.91
260	2.28	0.79	6.30	9.20	4.18	4.18	0.58	3.0×10^{-8}	0.48	0.741	488k	0.89
240	2.18	0.80	6.80	9.82	4.31	4.30	0.54	1.5×10^{-8}	0.48	0.708	1M	0.86
220	1.94	0.80	7.50	11.00	4.50	4.35	0.49	2.8×10^{-9}	0.44	0.752	421k	0.89
200	1.89	0.83	7.50	11.82	4.47	4.47	0.45	8.5×10^{-10}	0.44	0.724	2M	0.86
180	1.64	0.83	8.14	13.46	4.46	4.48	0.40	8.0×10^{-10}	0.48	0.689	7M	0.84
160	1.28	0.88	8.76	15.00	4.86	4.72	0.35	2.0×10^{-10}	0.48	0.623	50M	0.81

respectively. The obtained ideality factor deviates from the unity and starts to decrease almost linearly with decreasing the temperature. Similar results were also reported for pure bulk ZnO [16]. Mtangi and his co-authors found that the value of n initially increased with decreasing the temperature and then began to decrease with a further decrease in the temperature. Erdal and his co-authors [48] reported a decrease in the value of n with a further decrease in the temperature (400 K to 150 K) in the fabricated purely Ti/AlO_2/n-Si- and Cu-doped Al/$CuTiO_2$/n-Si Schottky diode devices. This decrease in n could be due to the change in the current transport mechanisms from thermionic emission at (280 to 320 K) to generation recombination at (180 to 260 K) and only recombination process below 160 K [49]. Interestingly, in the temperature range 320–240 K, the value of n is found to deviate from unity being greater than two however, with further decrease in temperature, it becomes close to unity (see Fig. 4a). The deviation of n from the ideal value could be due to the effect of doping, series resistance, interface states, and voltage drop across metal–semiconductor junction [30, 50, 51]. Moreover, the image force and/or barrier inhomogeneity, and the Ce and Sm co-doping could also be responsible for this deviation [30, 50, 51]. The value of Schottky barrier height is found to increase with decreasing temperature as depicted in Fig. 4b. A similar increase in Φ_{B_0} with temperature was also seen in the GaAs Schottky diodes [52–54]. The lowest

Table 3 Schottky diodes parameters of the Pt/ZnO:Ce,Sm/n-Si/Ti/Al devices evaluated using the thermionic emission ln I vs. V, Cheung and Nord method

T	ln I vs. V			$d(V)/d(\ln I)$		H(I)		Nord				
	n	Φ_{B_0}	R_s	n	R_s	R_s	Φ_{cheu}	I_0(A)	V_0	$F(V_0)$	R_s	Φ_N
(K)		(eV)	(Ω)	n	(Ω)	(Ω)	(eV)	I_0(A)	(V)	V	(kΩ)	(eV)
320	2.31	0.815	244	6.86	237	238	0.574	6.0×10^{-7}	0.33	0.776	31.71	0.858
300	2.41	0.789	242	6.92	246	255	0.527	4.0×10^{-7}	0.36	0.752	38.84	0.846
280	2.45	0.765	243	7.00	259	264	0.497	3.7×10^{-7}	0.42	0.728	35.22	0.844
260	2.68	0.732	243	7.10	275	277	0.465	2.2×10^{-7}	0.45	0.704	20.85	0.831
240	2.81	0.703	243	7.34	280	291	0.425	2.0×10^{-7}	0.51	0.680	19.35	0.829
220	3.24	0.664	250	7.96	265	308	0.366	4.4×10^{-7}	0.63	0.607	22.62	0.745
200	3.60	0.627	256	7.25	349	324	0.380	2.7×10^{-7}	0.66	0.581	25.88	0.729
180	4.25	0.582	262	7.87	342	341	0.332	1.0×10^{-6}	0.81	0.512	12.80	0.659
160	4.72	0.536	267	11.41	350	360	0.217	1.5×10^{-6}	1.00	0.481	24.30	0.647

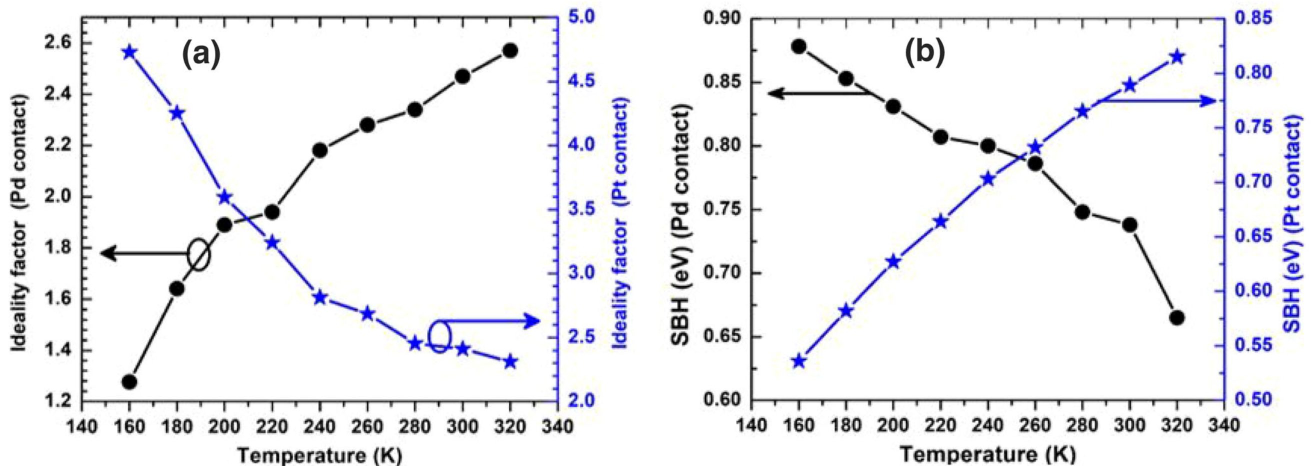

Fig. 4 **a** The ideality factor and **b** barrier height of Pd and Pt Schottky contacts as a function of temperature

value obtained for Pd-based ZnO Schottky diode is 0.665 eV at 320 K and the highest is 0.878 eV at 160 K. This increase in Φ_{B_0} with decreasing temperature contradicts the negative temperature coefficient of resistance in the group $II - -V$ semiconductor [55]. The trend in Φ_{B_0} with temperature could be due to the effect of Ce and Sm co-doping. Interestingly, as is clear in Fig. 4b (solid circle) in the temperature range of 220–160 K, Φ_{B_0} increased linearly with decreasing the temperature. As we know, the value of the Schottky barrier height for an ideal diode should increase with decreasing temperature, and only charge carriers with high energy will overcome the barrier height. This increase in Φ_{B_0} with decreasing the temperature indicates that the fabricated Schottky diodes based on Pd contact are an ideal diode.

For Pt-based Schottky diodes, the parameters from the I–V characteristics are presented in Table 3. Figure 4a (blue solid star) indicates an increase in n with decreasing the temperature. It is clear that the values of n increased and become greater than one at lower temperatures. As stated in the previous section, the same reason for the deviation of n from the ideal value of the diodes will also apply here. Adding to these, the defects that may be introduced by e-beam could also be responsible for this deviation from the ideal value ($n = 1$). Figure 4b (blue solid star) indicates a linear decrease in Φ_{B_0} with decreasing temperature. This trend may be explained by the Gaussian distribution [56]. This distribution of the barrier height could be due to the presence of a

number of surface states and the formation of an interfacial layer at the interface between ZnO: Ce, Sm, and Pt. This interfacial layer in turn produced a barrier height for the charge carriers to move from semiconductors to metals [57]. Moreover, the presence of an oxides layer could also be responsible for the decrease in the value of Φ_B [58]. Notably, the behavior of the Schottky barrier height in the case of Pt is unlike that of Pd is found to decrease with decreasing temperature, and only charge carriers with high energies will be able to overcome lower barrier height which means. This suggests that the current transport will be predominantly flowing through areas (patches) that have a lower barrier height. Therefore, the Schottky barrier height will become smaller and the ideality factor will be larger with a further decrease in temperature. Furthermore, this decrease in the Schottky barrier height with decreasing the temperature in the fabricated Pt-based Schottky diode devices could be attributed to barrier height inhomogeneities [59, 60].

It is well known that in a good Schottky diode device, the value of the barrier height may not be similar over the same contact area because of the difference in the thickness of the interfacial layer and also the non-uniformity of the interfacial charges. As a result, different types of distribution functions in describing the barrier inhomogeneities have been suggested, for example, log-normal [61] and Gaussian [62]. Since our deposited films with spin coater were not smooth over the substrate, and hence, the deposited Schottky contact thickness is different over the same area, which implies barrier height fluctuation. Therefore, assuming the Gaussian distribution of the barrier height is of reasonable with $\bar{\Phi}_b$ (mean barrier height) and standard deviation σ_s over the Schottky diode contact. To see the homogeneity of this Schottky barrier height, a correlation plot between n and Φ_{B_0} is shown in Fig. 5a. It is worth noting that the decrease in the barrier height is caused by the existence of a surface that can be analyzed using two Gaussian distribution modules [60]. The barrier height according to this model is expressed as follows [61, 63–65]:

$$\Phi_{\mathrm{eff}} = \bar{\Phi}_b - q\frac{\sigma_s^2}{2kT}, \tag{4}$$

where $\bar{\Phi}_b$ (eV) is the zero bias mean barrier height, and σ_s is the standard deviation of the Schottky barrier height distribution in eV. σ_s is, therefore, the measure of the barrier homogeneity (i.e., the larger value indicates that the barrier is more inhomogeneous). According to Eqn. 4, a plot of Φ_{B_0} versus 1/2kT should yields a straight with the slope giving σ_s at zero bias and intercept determining the barrier height at applied zero bias as well. The value of $\bar{\Phi}_b$ and σ_s can be obtained by fitting curves to the data in Fig. 5b using Eqn. 4, where the intercept represents $\bar{\Phi}_b$ and the slope gives -σ_s^2. Interestingly, a plot of Φ_{B_0} versus 1/2kT shows two straight lines in different temperature ranges 240–320 K (high) and 160–220 K (low) (see Fig. 5 (b)) corresponding to two Gaussian distribution of the barrier height. The obtained values of ($\bar{\Phi}_b$ and σ_s) from the fit in high temperature ranges found to be (1.15 and 0.136) (eV), respectively, while in the low temperature range, found to be (1.00 and 0.123) (eV). As can be seen that, the values of $\bar{\Phi}_0$ and σ_s at higher temperature are larger than the one obtained at lower temperature. This may be due to the existence of large interface inhomogeneity in the contact area.

4.2.1 *Cheung-Cheung function*

The Schottky diodes parameters extracted from the thermionic emission theory presented in Table 2 and 3 were obtained without taking the effect of the series resistance into account. Therefore, more accurate methods are needed to obtain the diode parameters where the effect of $R\ s$ will be considered. Usually, the effect of R_s is modeled by considering resistor in series with diode in which the current I flows. Cheung-Cheung method [66] is used to obtain diodes parameters from the I–V characteristics in the forward bias using the following equations:

$$\frac{dV}{d(lnI)} = n\frac{k_\beta T}{q} + IR_s\,, \tag{5}$$

$$H(I) = V - \left(n\frac{k_\beta T}{q}\right) ln\left(\frac{I}{AA^*T^2}\right), \tag{6}$$

$$H(I) = n\Phi_{cheu} + IR_s\,. \tag{7}$$

Figure 6 and 7 demonstrate the $dV/d(\ln I)$ and $H(I)$ vs I plot of the fabricated Pd- and Pt-based Schottky diode devices in the temperature range 320–160 K, respectively. The values of R_s and n are obtained from the linearity of $dV/d(\ln I)$ vs I as the slope and intercept, respectively. A plot of $H(I)$ vs I shown in Fig. 6 and 7 is obtained by substituting the values of

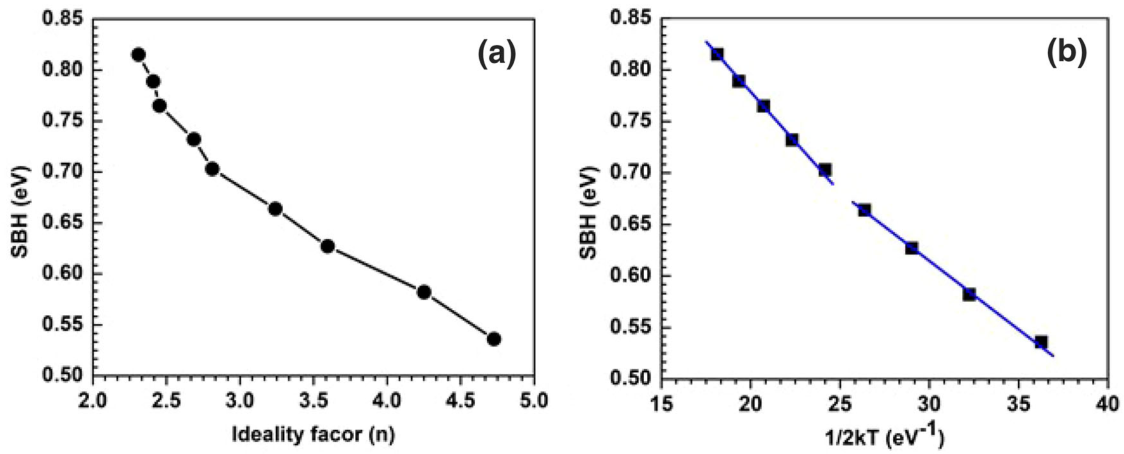

Fig. 5 The Schottky barrier height versus ideality factor (**a**) and inverse temperature (**b**) of Pt/ZnO:Ce,Sm/n-Si/Ti/Al Schottky diode devices, respectively

Fig. 6 Plots of $dV/d(\ln I)$ and $H(I)$ vs I for Pd/ZnO:Ce,Sm/n-Si/AuSb Schottky diodes devices

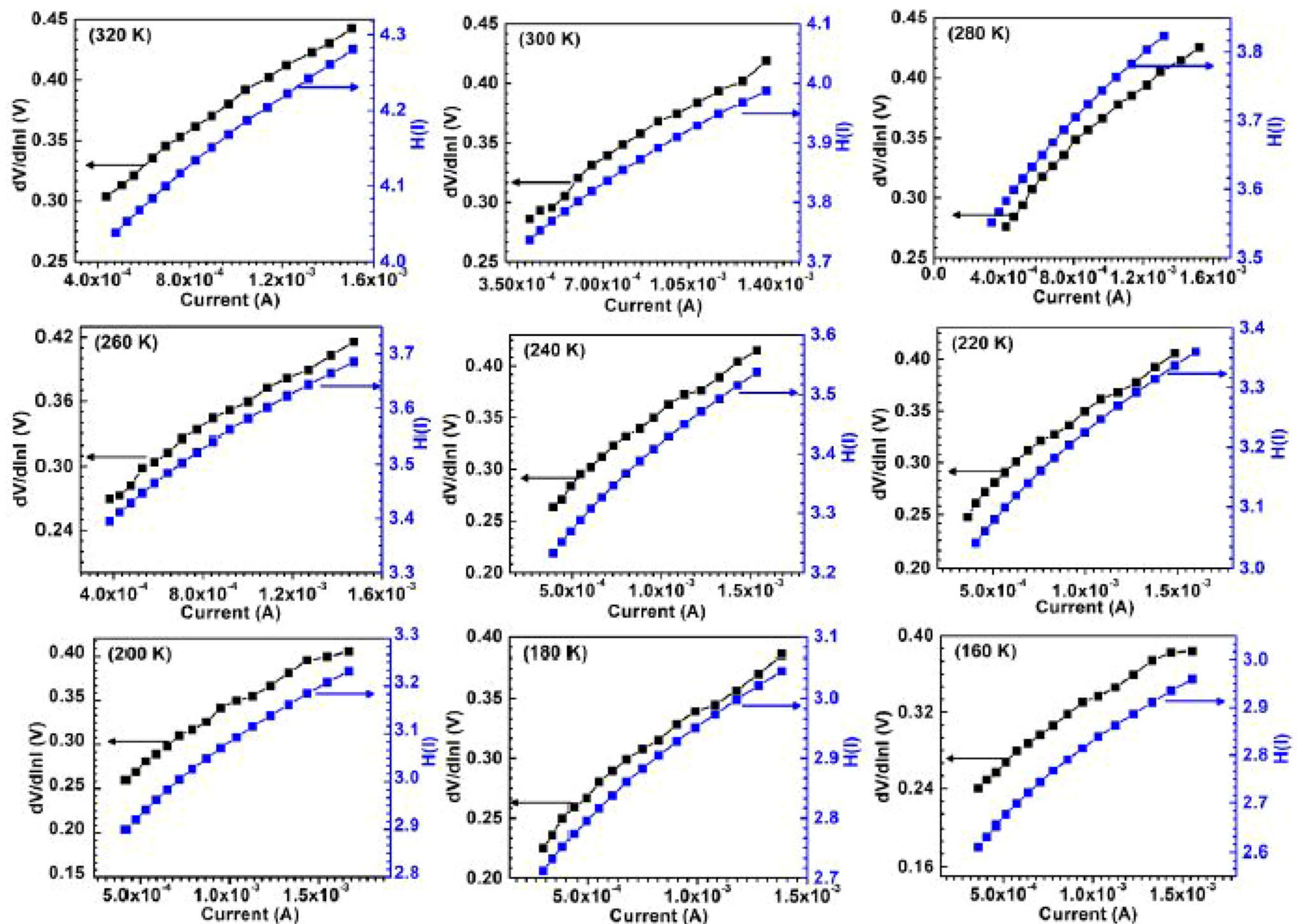

Fig. 7 Plots of $dV/d(\ln I)$ and $H(I)$ vs I for Pt/ZnO:Ce,Sm/n-Si/Ti/Al Schottky diodes devices

R_s and n in Eqn. 7. By using Eqn. 7 and a plot of $H(I)$ vs I, R_s and $\Phi_{B_{cheu}}$ are obtained as the slope and intercept, respectively. Evaluated values of R_s, n and $\Phi_{B_{cheu}}$ for both Pd- and Pt-based Schottky diode devices are tabulated in Tables 2 and 3.

In the case of Pd-based Schottky diode devices, it is observed that the values of n obtained using Cheung method are much larger compared with those obtained using the conventional thermionic emission theory. It is also seen that n increased with decreasing temperature. This opposite to the trend seen when using $\ln I$ vs V. This could be attributed to the presence of high series resistance, barrier inhomogeneity, and interface states. It is also observed that the values of R_s and obtained using Eqn. 5 and Eqn. 7 are in good agreement with each others, indicating the consistency of Cheung-Cheung methods. However, these values are slightly differ from those obtained with conventional thermionic theory when temperature is below 280 K ($\approx$ 40%) and could be attributed to the different approximations methods used to calculate R_s. Moreover, the trend of Φ_{cheu} obtained using Cheung-Cheung shows a decrease with decreasing the temperature differs from that obtained with $\ln I$ vs V. The decrease could be attributed to the existence of barrier inhomogeneity and also the effect of R_s.

For Pt-based Schottky diode devices, it is seen that both n and $\Phi_{B_{cheu}}$ obtained using Cheung-Cheung method showed a trend similar to that trend when using $\ln I$ vs V. Also, the value of n is much higher when compared with those ones obtained using $\ln I$ vs V, and this can also be attributed to the presence of barrier inhomogeneity discussed earlier. Interestingly, the values of R_s extracted using both conventional thermionic theory and Cheung-Cheung methods agree with each other (see Table 3). The reason for the increase in n and R_s evaluated with decreasing the temperature could be attributed to the

interface states and also the two Gaussian distribution in the barrier height discussed earlier.

4.2.2 Nord Function

The Schottky diode parameters, i.e., series resistance and barrier heights, were also obtained using the modified Nord's function that was developed by Bohlin and is expressed as follows [67]:

$$F(V) = \frac{V}{\gamma} - \frac{kT}{q}\ln\left(\frac{I(V)}{AA^*T^2}\right), \tag{8}$$

where $I(V)$ represents the current obtained from the I–V characteristics curve, and γ is an integer number greater than the ideality factor value. A plot of $F(V)$ vs V for both Pd and Pt-based Schottky diodes in the temperature range from 320–160 K is shown in Fig. 8. The values of R_s and Φ_N for Pd and Pt-based Schottky diode devices tabulated in Table 2 and 3 are obtained from Fig. 8 using the following equations [67]:

$$R_s = \frac{\gamma - n}{I_0}, \tag{9}$$

$$\Phi_N = F(V_0) + \left[\frac{V_0}{\gamma} - \frac{kT}{q}\gamma\right], \tag{10}$$

where $F(V_0)$ represents the minimum value in Fig. 8, V_0 is corresponding voltage of $F(V_0)$ and I_0 is current related to V_0. For Pd-based Schottky diode devices, it is observed that the values R_s increased drastically with decreasing temperature, while Φ_N decreased (see Table 2). This increase in the values of R_s could be attributed to the decrease of charge carriers in the fabricated Schottky diode devices due to the effect of Ce and Sm co-doping. Similar decrease in the value of charge carriers was also observed in our previous work when ZnO was co-doped with Ce and Al [30]. Moreover, calculated values of Φ_N were higher than those obtained with Cheung-Cheung methods. The trend was also opposite to that seen with conventional thermionic emission theory, and this could be due to the effect of the series resistance.

For Pt-based Schottky diodes devices, it is also observed that the both the values R_s and Φ_N decreased as the temperature decreased (see Table 3). It is noted that the values of R_s and Φ_N were larger than those ones obtained from Cheung-Cheung methods, and Φ_N agrees with Φ_{B_0} obtained using conventional thermionic emission theory. This decrease in the value of R_s could be attributed to the increasing in the charge carriers with decreasing temperature [68]. The decrease in the value of Φ_N might be due to the inhomogeneity in barrier height. Interestingly, for all fabricated devices, there are differences in the series resistance and Schottky barrier heights obtained using Cheung-Cheung and Norde methods. These differences could be attributed to fact that Cheung-Cheung is applied in the non-linear region in the high-voltage forward bias, while Norde is applied to the whole I–V curve in forward bias.

4.2.3 Current transport mechanism

To study the current transport mechanisms in the fabricated Ce and Sm-co-doped ZnO based on Pd and Pt Schottky diode devices in the temperature

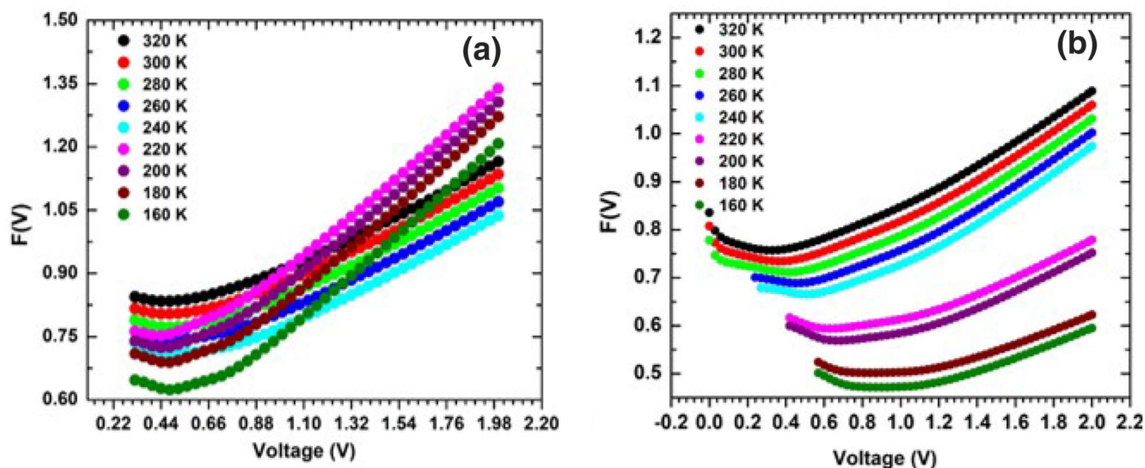

Fig. 8 (Color online) Plots of F(V) vs V for the fabricated Ce and Sm-co-doped ZnO thin films based on **a** Pd and **b** Pt in the temperature range 320 to 160 K

range 320 to 160 K, a logarithmic plot in the forward bias of current–voltage (i.e., log I vs log V) is shown in Fig. 9a and 9b. As can be seen clearly in Fig. 9, three distinct linear regions are identified as follows: region I, region II, and region III, indicating three different transport mechanisms that controlled the current behavior in the fabricated Schottky diode devices. In general, if there are deep traps presence at the interface, the current transport behavoir will be affected resulting in changing the value of the slopes obtained from the logarithmic plots of $I--V$. The extracted values for the slopes in the three different regions are tabulated in Table. 4 for Pd and Pt-based Schottky diode devices.

In region I (lower voltage V < 0.25 V) for both Pd and Pt-based Schottky diode devices, the current is linearly dependent to the applied voltage (i.e., $I \sim V$). It is noted that the slopes obtained in this region for Pd and Pt Schottky diode devices from 320 K to 220 K are close to unity, indicating that the current transport mechanism is governed by an ohmic conduction mechanism. However, at a temperature less than 220 K, the value becomes 2, suggesting that the presence of another transport mechanism is alongside the ohmic conduction mechanism (see Table 4). Also, in this region and due to lower voltage bias, the injection of charge carriers from electrode to semiconductor materials is reduced. In region II (moderate voltage, 0.25<V<0.9 V), the current increased exponentially following the relation $I \sim e^{aV}$, where a represents the injection efficiency constant. The higher value of a is indicative of a higher carrier injection and the lower value of a indicates a decrease in the carriers due to surface states [69]. The slope for Pd and Pt-based Schottky diode devices in this region shows an increase with decreasing the temperature as can be seen in Table 4. This increase with decreasing temperature indicates that more carriers are injected into the junction between metal and semiconductor. The current transport mechanism in this region is controlled by space-charge-limited current (SCLC) and trap-filled voltage (V_{TFL}) mechanisms. The latter one is explained as a voltage where the traps are filled with carriers [70, 71]. When the applied voltage increased, the number of injected charge carriers also increased resulting in traps being filled with carriers [72]. In region III (high voltage, 0.9<V<2.0 V), the current was found to increase following the relation $I \sim V^L$, where L is constant represented by the slope in this region. The slope in this region was found to be in the range of 4.0–5.0 and 4.7–9.4 for Pd and Pt-based Schottky diode devices, respectively (see Table 9). The obtained value of the slopes for both Pd and Pt-based Schottky diode devices was found to be greater than two, indicating that the current transport mechanism is controlled by space-charge-limited current (SCLC) [73, 74]. The SCLC mechanism is controlled by the present of traps in band gap of Ce and Sm-co-doped ZnO materials [73]. In general, the SCLC occurs when the equilibrium charge concentration is insignificant compared to the injected charge, and because of that, a space charge region near the electrode injection will be formed [73].

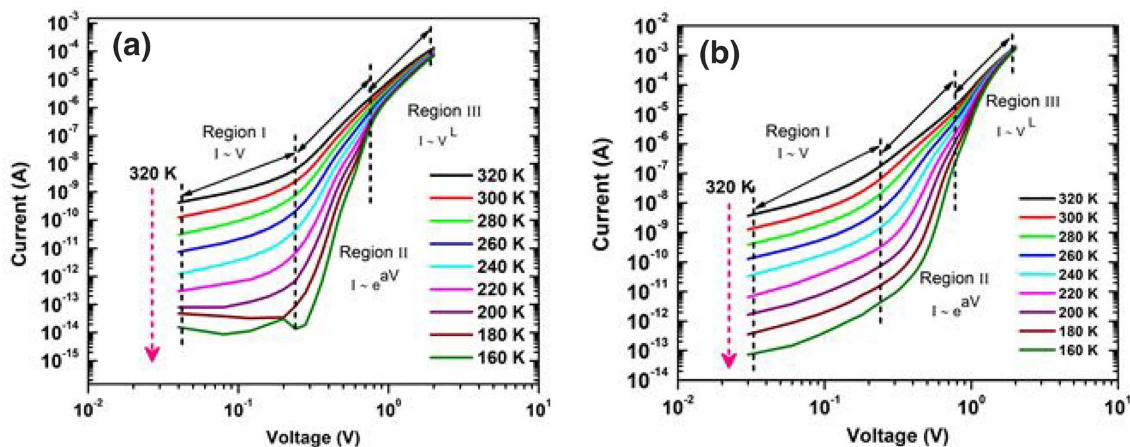

Fig. 9 The transport mechanism of **a** Pd/ZnO:Ce,Sm/n-Si/AuSb and **b** Pt/ZnO:Ce,Sm/n-Si/Ti/Al Schottky diode devices in the temperature range 320 to 160 K

Table 4 Current transport mechanism's slope of the fabricated Pd and Pt Schottky diode devices in the temperature range 320–160 K

Temperature	Slope (Pd-based Schottky didoes)			Slope (Pd-based Schottky didoes)		
(K)	Region I	Region II	Region III	Region I	Region II	Region III
320	1.5	5.4	4.2	1.4	3.3	4.7
300	1.4	5.8	4.4	1.4	3.8	4.8
280	1.3	5.8	5.0	1.4	4.5	5.0
260	1.3	7.5	5.0	1.5	5.0	5.7
240	1.4	8.6	5.4	1.6	6.0	6.0
220	1.3	10.0	5.0	1.7	7.5	6.4
200	2.0	11.7	5.3	2.0	9.6	7.0
180	–	13.5	5.2	2.0	11.6	8.0
160	–	17.0	5.4	2.0	13.4	9.4

5 Conclusion

We have successfully fabricated Schottky diode devices based on Ce and Sm-co-doped ZnO thin films using the sol–gel spin-coating technique with the structure Pd/CeSmZnO/n-Si/AuSb and Pt/CeSmZnO/n-Si/Ti/Al. The structural properties studied with XRD revealed that the nature of the prepared films was polycrystalline in nature with some preferred growth orientation along the (002) plane. The *I*–*V* characteristic of the fabricated Schottky diode devices based on Pd and Pt Schottky contacts investigated in the temperature range 320–160 K manifests very good Schottky diode behavior. The rectification orders for Pd and Pt-based Schottky diode devices at ±2 V were found to be nine and 10 orders of magnitude, respectively. With decreasing the temperature, the ideality factor was found to decrease for Pd-based device with the lowest value obtained 1.3; however, for Pt-based device, the ideality factor was found to increase with decreasing temperature. The Schottky barrier heights obtained for Pd devices were found to increase with a decrease in temperature, while those of the Pt devices decreased. The behavior of the Schottky barrier heights in the case of Pt was found to differ from the ideal Schottky diode behavior and is attributed to the inhomogeneity in the barrier that was found to have two Gaussian distribution in the barrier height. Moreover, alongside the thermionic emission theory, Schottky barrier diode parameters were also analyzed with Cheung-Cheung and the modified Nord function. Furthermore, the current transport mechanism for both fabricated Schottky diode devices in the temperature range 320–160 K was found to be Ohmic at low voltages, trap-filled voltage at moderate voltages, and space-charge-limited current at high voltages.

Acknowledgements

The authors would like to thank Mr Mojahid Hassan and Mr Babiker Jafar (both are PhD students) for their help with XRD measurements at the University of Free state. The authors would like also to thank Prof H. Swart for allowing us to use XRD machine in the Physics department at the University of Free State.

Author contributions

MA: prepared the samples, fabricated the devices, acquired and analyzed the data, writing the original draft of the manuscript. WM: supervision, reviewing and editing the manuscript. JN: supervision, reviewing and editing the manuscript and approving the final draft.

Funding

Open access funding provided by University of Pretoria. This work is supported by the South African National Research Foundation (NRF) grant no: 91550 and 111744. The opinions, findings, and conclusion are those of the authors, and NRF accepts no responsibility whatsoever in this regard.

Data availability

Data will be made available on request.

Declarations

Conflict of interest The authors declare that they have no known competing financial interests or personal relationship that could have appeared to influence the work reported in this paper.

Ethical approval and consent to participate Not applicable

Consent for publication Not applicable

Open Access This article is licensed under a Creative Commons Attribution 4.0 International License, which permits use, sharing, adaptation, distribution and reproduction in any medium or format, as long as you give appropriate credit to the original author(s) and the source, provide a link to the Creative Commons licence, and indicate if changes were made. The images or other third party material in this article are included in the article's Creative Commons licence, unless indicated otherwise in a credit line to the material. If material is not included in the article's Creative Commons licence and your intended use is not permitted by statutory regulation or exceeds the permitted use, you will need to obtain permission directly from the copyright holder. To view a copy of this licence, visit http://creativecommons.org/licenses/by/4.0/.

References

1. R. Vispute, V. Talyansky, S. Choopun, R. Sharma, T. Venkatesan, M. He, X. Tang, J. Halpern, M. Spencer, Y. Li et al., Heteroepitaxy of ZnO on GaN and its implications for fabrication of hybrid optoelectronic devices. Appl. Phys. Lett. **73**(3), 348–350 (1998)
2. K. Chung, C. Lee, G. Yi, Transferable gan layers grown on ZnO-coated graphene layers for optoelectronic devices. Science **330**(6004), 655–657 (2010)
3. A. El Hajj, B. Lucas, M. Chakaroun, R. Antony, B. Ratier, M. Aldissi, Optimization of ZnO/Ag/ZnO multilayer electrodes obtained by Ion Beam Sputtering for optoelectronic devices. Thin Solid Films **520**(14), 4666–4668 (2012)
4. E.M. Hashem, M.A. Hamza, A.N. El-Shazly, M.F. Sanad, M.M. Hassan, S.O. Abdellatif, Investigating the UV absorption capabilities in novel Ag@ RGO/ZnO ternary nanocomposite for optoelectronic devices. Nanotechnol. **32**(8), 085701 (2020)
5. D. Hwang, S. Kang, J. Lim, E. Yang, J. Oh, J. Yang, S. Park, p-ZnO/n-GaN heterostructure ZnO light-emitting diodes. Appl. Phys. Lett. **86**(22), 222101 (2005)
6. T.Ortiz, C. Conde, T.M. Khan, B.H, Thickness uniformity and optical/structural evaluation of RF sputtered ZnO thin films for solar cell and other device applications, Appl. Phys. A 123 (4) 1–6 (2017)
7. D. Zhang, Z. Wu, X. Zong, Metal-organic frameworks-derived zinc oxide nanopolyhedra/S, N: graphene quantum dots/polyaniline ternary nanohybrid for high-performance acetone sensing. Sens. Actuators B: Chemi. **288**, 232–242 (2019)
8. A.A. Farrag, M.R. Balboul, Nano ZnO thin films synthesis by sol-gel spin coating method as a transparent layer for solar cell applications. J. Sol-Gel Sci. Techn. **82**(1), 269–279 (2017)
9. R. Vinodkumar, I. Navas, S. Chalana, K. Gopchandran, V. Ganesan, R. Philip, S. Sudheer, V.M. Pillai, Highly conductive and transparent laser ablated nanostructured Al: ZnO thin films. Appl. Surf. Sci. **257**(3), 708–716 (2010)
10. H. von Wenckstern, G. Biehne, R.A. Rahman, H. Hochmuth, M. Lorenz, M. Grundmann, Mean barrier height of Pd Schottky contacts on ZnO thin films. Appl. Phys. Lett. **88**(9), 092102 (2006)
11. Y. Nam, I. Hwang, S. Oh, S. Lee, K. Lee, S. Hong, J. Kim, T. Choi, B. Ho Park, Switchable Schottky diode characteristics induced by electroforming process in Mn-doped ZnO thin films, Appl. Phys. Lett. 102 (16) 162105 (2013)
12. A.B. Yadav, A. Pandey, S. Jit, Pd Schottky contacts on sol-gel derived ZnO thin films with nearly ideal Richardson constant. IEEE Electron Device lett. **35**(7), 729–731 (2014)
13. R. Gayen, R. Paul, S. Biswas, Schottky enabled enhanced UV detection by graphene oxide composited transparent ZnO thin films. Appl. Surf. Sci. **533**, 147149 (2020)
14. O. Goktas, N. Koksal, O. Kaplan, A. Yildiz, Sol-gel prepared ZnO: Al thin films for heterojunction diodes. J. Mater. Sci. Mater. Electron. **32**(6), 7791–7800 (2021)
15. X. Zhao, J. Liang, J. Sun, J. Guo, S. Dursun, K. Wang, C.A. Randall, Cold sintering ZnO based varistor ceramics with controlled grain growth to realize superior breakdown electric field. J. Eur. Ceram. Soc. **41**(1), 430–435 (2021)
16. W. Mtangi, F. Auret, C. Nyamhere, P.J. Van Rensburg, M. Diale, A. Chawanda, Analysis of temperature dependent I-V measurements on Pd/ZnO schottky barrier diodes and the determination of the Richardson constant. Phys. B: Cond. Matt. **404**(8–11), 1092–1096 (2009)
17. K. Khojier, Preparation and investigation of Al-doped ZnO thin films as a formaldehyde sensor with extremely low detection limit and considering the effect of Rh. Mater. Sci. Semicond. Process. **121**, 105283 (2021)

18. A. Saboor, S.M. Shah, H. Hussain, Band gap tuning and applications of ZnO nanorods in hybrid solar cell: Ag-doped verses Nd-doped ZnO nanorods. Mater. Sci. Semicond. Process. **93**, 215–225 (2019)
19. N. Ali, B. Singh, V. AR, S. Lal, C. Yadav, K. Tarafder, S. Ghosh, Ferromagnetism in Mn-doped ZnO: A joint theoretical and experimental study, J. Phys. Chem. C 125 (14) 7734–7745 (2021)
20. P. Chithira, T.T. John, Correlation among oxygen vacancy and doping concentration in controlling the properties of cobalt doped ZnO nanoparticles. J. Magn. Magn. Mater. **496**, 165928 (2020)
21. M.M. Ahmed, W.Z. Tawfik, M. Elfayoumi, M. Abdel-Hafiez, S. El-Dek, Tailoring the optical and physical properties of La doped ZnO nanostructured thin films. J. Alloy Compd. **791**, 586–592 (2019)
22. T.K. Pathak, E. Coetsee-Hugo, H. Swart, C. Swart, R. Kroon, Preparation and characterization of Ce doped ZnO nanomaterial for photocatalytic and biological applications. Mater. Sci. Engn: B **261**, 114780 (2020)
23. D. Ali, M. Butt, I. Muneer, M. Farrukh, M. Aftab, M. Saleem, F. Bashir, A. Khan, Synthesis and characterization of sol-gel derived La and Sm doped ZnO thin films: A solar light photo catalyst for methylene blue. Thin Solid Films **679**, 86–98 (2019)
24. V. Kumar, O. Ntwaeaborwa, H. Swart, Effect of oxygen partial pressure during pulsed laser deposition on the emission of Eu doped ZnO thin films. Phys. B Condens. Matter. **576**, 411713 (2020)
25. E.R. López-Mena, O. Ceballos-Sanchez, T. Hooper, G. Sanchez-Ante, M. Rodríguez-Muñoz, J.A. Renteria-Salcedo, A. Elías-Zuñiga, A. Sanchez-Martinez, The effect of Yb doping on ZnO thin films obtained via a low-temperature spin coating method. J. Mater. Sci. Mater. Electron. **32**(1), 347–359 (2021)
26. R. Zamiri, A. Lemos, A. Reblo, H.A. Ahangar, J. Ferreira, Effects of rare-earth (Er, La and Yb) doping on morphology and structure properties of ZnO nanostructures prepared by wet chemical method. Ceram. Int. **40**(1), 523–529 (2014)
27. D. Alsebaie, W. Shirbeeny, A. Alshahrie, M.S. Abdel-Wahab, Ellipsometric study of optical properties of Sm-doped ZnO thin films Co-deposited by RF-Magnetron sputtering. Optik **148**, 172–180 (2017)
28. M. Ahmed, W.E. Meyer, J.M. Nel, Structural, optical and electrical properties of the fabricated schottky diodes based on ZnO, Ce and Sm doped ZnO films prepared via wet chemical technique. Mater. Rese. Bull. **115**, 12–18 (2019)
29. M.A. Ahmed, L. Coetsee, W.E. Meyer, J.M. Nel, Influence (Ce and Sm) co-doping ZnO nanorods on the structural, optical and electrical properties of the fabricated Schottky diode using chemical bath deposition. J. Alloy Compd. **810**, 151929 (2019)
30. M. Ahmed, W.E. Meyer, J.M. Nel, Effect of (Ce, Al) co-doped ZnO thin films on the Schottky diode properties fabricated using the sol-gel spin coating. Mater. Sci Semicond Process. **103**, 104612 (2019)
31. R.T. Tung, Recent advances in Schottky barrier concepts. Mater. Sci. Eng. R Rep. **35**(1–3), 1–138 (2001)
32. N. Yildirim, H. Korkut, A. Türüt, Temperature-dependent Schottky barrier inhomogeneity of Ni/n-GaAs diodes, Eur. Phys. J. Appl. Phys. 45 (1)
33. Ç. Güçlü, A. Özdemir, D. Aldemir, Ş Altındal, The reverse bias current-voltage-temperature (I-V-T) characteristics of the (Au/Ti)/Al_2O_3/n-GaAs Schottky barrier diodes (SBDs) in temperature range of 80–380 K. J. Mater. Sci. Mater. Electron. **32**(5), 5624–5634 (2021)
34. K. Reddy, H. Gopalaswamy, P. Reddy, R. Miles, Effect of gallium incorporation on the physical properties of ZnO films grown by spray pyrolysis. J. Cryst. Growth **210**(4), 516–520 (2000)
35. J.Y. Park, D.J. L, S.S. Kim, Size control of ZnO nanorod arrays grown by metalorganic chemical vapour deposition, Nanotechnol. 16 (10) 2044 (2005)
36. D.C. Look, D. Reynolds, C. Litton, R. Jones, D. Eason, G. Cantwell, Characterization of homoepitaxial p-type ZnO grown by molecular beam epitaxy. Appl. Phys. Lett. **81**(10), 1830–1832 (2002)
37. B. Jin, S. Im, S.Y. Lee, Violet and UV luminescence emitted from ZnO thin films grown on sapphire by pulsed laser deposition. Thin Solid Films **366**(1–2), 107–110 (2000)
38. M. Kamalasanan, S. Chandra, Sol-gel synthesis of ZnO thin films. Thin solid films **288**(1–2), 112–115 (1996)
39. G. Vijayaprasath, R. Murugan, G. Ravi, T. Mahalingam, Y. Hayakawa, Characterization of dilute magnetic semiconducting transition metal doped ZnO thin films by sol-gel spin coating method. Appl. Surf. Sci. **313**, 870–876 (2014)
40. A. Zak, N. Aziz, A.M. Hashim, F. Kordi, XPS and UV-vis studies of Ga-doped zinc oxide nanoparticles synthesized by gelatin based sol-gel approach. Ceram. Int. **42**(12), 13605–13611 (2016)
41. A. Boukhari, B. Deghfel, A. Mahroug, R. Amari, N. Selmi, S. Kheawhom, A.A. Mohamad, Thickness effect on the properties of Mn-doped ZnO thin films synthesis by sol-gel and comparison to first-principles calculations. Ceram. Int. **47**(12), 17276–17285 (2021)
42. H.T. Danga, F.D. Auret, S.M. Tunhuma, E.Omotoso, E.Igumbor, W.E. Meyer, Electrical characterization of electron beam exposure induced defects in epitaxially grown n-type silicon, in: AIP Conference Proceedings, Vol. 2109, AIP Publishing LLC, 2019, p. 080003

43. R. Balboni, R. Lemos, E. Moura, C. Cholant, C. Azevedo, I. Caldeira, A. Gündel, W. Flores, A. Pawlicka, C. Avellaneda, Electrochemical, UV–Vis, and microscopical characteristics of sol–gel CeO_2: V_2 O_5 thin film, J. Mater. Sci.: Mater. Electron. 29 (19) 16911–16920 (2018)
44. P. Scherrer, Bestimmung der Grösse und der inneren Struktur von Kolloidteilchen mittels Röntgenstrahlen. Nachr. Ges. Wiss zu Göttingen **26**, 98–100 (1918)
45. U. Holzwarth, N. Gibson, The Scherrer equation versus the'Debye-Scherrer equation'. Nat. Nanotechno. **6**(9), 534–534 (2011)
46. G. Murtaza, M. Iqbal, Y. Xu, I. Will, Z. Huang, Study of Sm-doped ZnO samples sintered in a nitrogen atmosphere and deposited on n-Si (1 0 0) by evaporation technique. J. Mag. Magn Mater. **323**(24), 3239–3245 (2011)
47. E. Rhoderick, R. Williams, M.-S. Contacts, 2nd edn, Clarendon, Oxford
48. M.O. Erdal, A. Kocyigit, M. Yıldırım, Temperature dependent current-voltage characteristics of Al/TiO_2/n-Si and Al/Cu: TiO_2/n-Si devices. Mater. Sci. Semicond. Process. **103**, 104620 (2019)
49. S.M. Sze, K.K. Ng, *Physics of Semiconductor Devices* (Wiley, New York, 2006)
50. L.J. Brillson, Y. Lu, ZnO Schottky barriers and ohmic contacts. J. Appl. Phys. **109**(12), 8 (2011)
51. N.S. Singh, L. Kumar, A. Kumar, S. Vaisakh, S.D. Singh, K. Sisodiya, S. Srivastava, M. Kansal, S. Rawat, T.A. Singh et al., Fabrication of zinc oxide/polyaniline (ZnO/PANI) heterojunction and its characterisation at room temperature. Mater. Sci. Semicond. Process. **60**, 29–33 (2017)
52. A. Gümüş, A. Türüt, N. Yalcin, Temperature dependent barrier characteristics of CrNiCo alloy Schottky contacts on n-type molecular-beam epitaxy GaAs. J. Appl. Phys. **91**(1), 245–250 (2002)
53. Ş Karataş, Ş Altındal, Temperature dependence of barrier heights of Au/n-type GaAs Schottky diodes. Solid State Electron. **49**(6), 1052–1054 (2005)
54. W. Mtangi, F.D. Auret, C. Nyamhere, P. Van-Rensburg, A. Chawanda, M. Diale, J.M. Nel, W.E. Meyer, The dependence of barrier height on temperature for Pd Schottky contacts on ZnO. Physica B **404**(22), 4402–4405 (2009)
55. B.G. Yacobi, *Semiconductor Materials: An Introduction to Basic Principles* (Springer, New York, 2003)
56. H. Li, D. He, Q. Zhou, P. Mao, J. Cao, L. Ding, J. Wang, Temperature-dependent Schottky barrier in high-performance organic solar cells. Sci. Rep. **7**(1), 1–10 (2017)
57. A. Karimov, D. Karimova, Three-junction Au/AlGaAs (n)/GaAs (p)/Ag photodiode. Mater. Sci. Semicond. Process. **6**(1–3), 137–142 (2003)
58. M. Özer, D. Yıldız, Ş Altındal, M. Bülbül, Temperature dependence of characteristic parameters of the Au/SnO_2/n-Si (MIS) Schottky diodes. Solid State Electron. **51**(6), 941–949 (2007)
59. A. Özdemir, A. Turut, A. Kökçe, The double gaussian distribution of barrier heights in Au/n-GaAs Schottky diodes from I-V-T characteristics. Semicond. Sci. Technol. **21**(3), 298 (2006)
60. D.K. Schroder, *Semiconductor Material and Device Characterization* (Wiley, New York, 2015)
61. S. Chand, J. Kumar, Evidence for the double distribution of barrier heights in Schottky diodes from I-V-T measurements. Semicond. Sci. Technol. **11**(8), 1203 (1996)
62. E. Dobročka, J. Osvald, Influence of barrier height distribution on the parameters of Schottky diodes. Appl. Phys. Lett **65**(5), 575–577 (1994)
63. Y. Song, R. Van Meirhaeghe, W. Laflere, F. Cardon, On the difference in apparent barrier height as obtained from capacitance-voltage and current-voltage-temperature measurements on Al/p-InP Schottky barriers. Solid State Electron. **29**(6), 633–638 (1986)
64. S. Chand, J. Kumar, Current-voltage characteristics and barrier parameters of Pd_2Si/p-Si (111) Schottky diodes in a wide temperature range. Semicond. Sci. Technol. **10**(12), 1680 (1995)
65. R. Badran, Y. Al-Hadeethi, A. Umar, S.H. Al-Heniti, B.M. Raffah, M.S. Ansari, A. Jilani, Temperature-dependent heterojunction device characteristics of n-ZnO nanorods/p-Si assembly. Mater. Express **10**(1), 29–36 (2020)
66. S. Cheung, N. Cheung, Extraction of Schottky diode parameters from forward current-voltage characteristics. Appl. Phys. Lett. **49**(2), 85–87 (1986)
67. K. Bohlin, Generalized Norde plot including determination of the ideality factor. J. Appl. Phys. **60**(3), 1223–1224 (1986)
68. A. Battal, D. Tatar, A. Kocyigit, B. Duzgun, Effect of substrate temperature on some properties doubly doped tin oxide thin films deposited by using spray pyrolysis. Mater. Focus **4**(6), 445–456 (2015)
69. S. Faraz, M. Willander, Q. Wahab, Interface state density distribution in Au/n-ZnO nanorods Schottky diodes, in: IOP Conference Series: Mater. Sci. Eng., Vol. 34, IOP Publishing, 2012, p. 012006
70. Ş Aydoğan, K. Çınar, H. Asıl, C. Coşkun, A. Türüt, Electrical characterization of Au/n-ZnO Schottky contacts on n-Si. J. Alloy Compd. **476**(1–2), 913–918 (2009)
71. A. Farag, W. Farooq, F. Yakuphanoglu, Characterization and performance of Schottky diode based on wide band gap semiconductor ZnO using a low-cost and simplified sol-gel spin coating technique. Microelectron. Eng. **88**(9), 2894–2899 (2011)

72. A. Jain, P. Kumar, S. Jain, V. Kumar, R. Kaur, R. Mehra, Trap filled limit voltage (V_{TFL}) and V^2 law in space charge limited currents. J. Appl. Phys. **102**(9), 094505 (2007)
73. M. Zhu, T. Cui, K. Varahramyan, Experimental and theoretical investigation of MEH-ppv based Schottky diodes. Microelectron. Eng. **75**(3), 269–274 (2004)
74. G. Amin, I. Hussain, S. Zaman, N. Bano, O. Nur, M. Willander, Current-transport studies and trap extraction of hydrothermally grown ZnO nanotubes using gold Schottky diode. Phys. Status Solidi A **207**(3), 748–752 (2010)

Publisher's Note Springer Nature remains neutral with regard to jurisdictional claims in published maps and institutional affiliations.